Local structure of (Ga,Fe)N and (Ga,Fe)N:Si investigated by x-ray absorption fine structure spectroscopy

Mauro Rovezzi* and Francesco D'Acapito
Italian Collaborating Research Group, BM08 "GILDA," ESRF, BP 220, F-38043 Grenoble, France
and Operative Group in Grenoble (OGG), Consiglio Nazionale delle Ricerche, INFM, BP 220, F-38043 Grenoble, France

Andrea Navarro-Quezada, Bogdan Faina, Tian Li, and Alberta Bonanni
Institute for Semiconductor and Solid State Physics, Johannes Kepler University, A-4040 Linz, Austria

Francesco Filippone and Aldo Amore Bonapasta
Istituto di Struttura della Materia (ISM), Consiglio Nazionale delle Ricerche, Via Salaria Km 29.5, CP 10, 00016 Monterotondo Stazione, Italy

Tomasz Dietl
Institute of Physics, Polish Academy of Sciences, PL-02-668 Warszawa, Poland
and Institute of Theoretical Physics, University of Warsaw, PL-00-681 Warszawa, Poland
(Received 26 February 2009; revised manuscript received 5 May 2009; published 28 May 2009)

X-ray absorption fine-structure (XAFS) measurements supported by *ab initio* computations within the density functional theory (DFT) are employed to systematically characterize Fe-doped as well as Fe- and Si-codoped films grown by metalorganic vapor-phase epitaxy. The analysis of extended-XAFS data shows that depending on the growth conditions, Fe atoms either occupy Ga substitutional sites in GaN or precipitate in the form of ϵ-Fe_3N nanocrystals, which are ferromagnetic and metallic according to the DFT results. Precipitation can be hampered by reducing the Fe content, by increasing the growth rate, or by codoping with Si. The near-edge region of the XAFS spectra provides information on the Fe charge state and shows its partial reduction from Fe^{+3} to Fe^{+2} upon Si codoping, in agreement with the Fe electronic configurations expected within various implementations of DFT.

DOI: 10.1103/PhysRevB.79.195209 PACS number(s): 61.05.cj, 61.46.Hk, 61.72.uj, 75.50.Pp

I. INTRODUCTION

It has been realized in recent years that a palette of nanocharacterization tools has to be employed in order to elucidate the origin of the surprising high-temperature ferromagnetism detected in a number of magnetically doped semiconductors and oxides.[1–5] The application of state-of-the-art analytic methods appears to reveal that the distribution of magnetic cations is generally highly nonuniform and that there is an ultimate relationship between the ion arrangement and the magnetic response of the system. In particular, randomly distributed localized spins account for the paramagnetic component of the magnetization, whereas regions with a high local density of magnetic cations are presumably responsible for ferromagnetic features. It has been found that the aggregation of magnetic ions—driven by a substantial contribution of open *d* shells to the bonding—leads either to crystallographic phase separation, i.e., to the precipitation of a magnetic compound or an elemental ferromagnet, or to the chemical phase separation into alternating regions with higher and lower concentration of magnetic cations, occurring without distorting the crystallographic structure. In the literature on diluted magnetic semiconductors (DMSs), this chemical phase separation is commonly referred to as spinodal decomposition,[1,6] independently of its microscopic origin.

There are already experimental indications that the above scenario applies to the case of (Ga,Fe)N fabricated by means of metalorganic vapor-phase epitaxy (MOVPE),[7–9] where—depending on the growth parameters and on the Fe concentration—Fe is either randomly distributed over cation sites or nonuniformly incorporated, showing spinodal decomposition or the presence of precipitates that have been identified as hexagonal ϵ-Fe_3N, according to synchrotron-radiation x-ray diffraction (XRD) and high-resolution transmission electron microscopy (HRTEM).[7,9] Moreover, by employing these nanoscale characterization methods it has been found that the aggregation of Fe cations is largely hampered by codoping with Si donors or Mg acceptors.[9]

In this work, we present results of x-ray absorption fine structure (XAFS) spectroscopy[10] carried out on (Ga,Fe)N and (Ga,Fe)N:Si samples. XAFS is a well-established tool in the study of semiconductor heterostructures and nanostructures[11] and has proven its power as a chemically sensitive local probe for the site identification of Mn/Fe dopants in *III-V* DMSs (Refs. 12–16) and of Mn-rich nanocolumns in Ge.[17] In the present case it allows us to obtain information on the local atom arrangement in the vicinity of Fe ions as well as on the Fe charge state, depending on the Fe concentration, growth conditions, and codoping. We then compare the experimentally determined bond lengths to the corresponding values expected from *ab initio* simulations. This combined experimental and computational effort makes it possible to identify the epitaxial parameters controlling the formation of ϵ-Fe_3N precipitates in (Ga,Fe)N. However, no presence of bonds specific to ϵ-Fe_3N has been detected in the

(Ga,Fe)N films codoped with Si. This finding provides a strong corroboration of the previous theoretical suggestions[18] and experimental observations[9] indicating that the alteration of the magnetic-ions valence by shallow impurities can hinder their aggregation and, therefore, extend the solubility range.

Our paper is organized as follows. In Sec. II A we present the relevant characteristics of the studied samples and we briefly recall the employed growth and doping procedures. The XAFS method and the analysis of both the extended x-ray absorption fine-structure (EXAFS) and x-ray absorption near-edge structure (XANES) regions of collected spectra are described in Sec. II B. The employed *ab initio* computation scheme is summarized in Sec. II C for the case of wurtzite (Ga,Fe)N and ϵ-Fe_3N. Section III contains an interpretation of the experimentally determined values of the bond lengths in the light of the theoretical results. As discussed in Sec. IV, this insight allows to quantify the relative concentration of Fe in the ϵ-Fe_3N precipitates depending on the growth conditions and codoping with Si. The main conclusions and outlook of our work are summarized in Sec. V.

II. EXPERIMENTAL

A. Samples production

The (Ga,Fe)N and (Ga,Fe)N:Si epilayers considered here are fabricated by MOVPE on *c*-plane sapphire substrates following the growth procedures and applying the *in situ* and *ex situ* characterization methods we have formerly reported for (Ga,Fe)N.[7] The total Fe concentration in the samples ranges from 4×10^{19} cm^{-3} to 3×10^{20} cm^{-3} for a Fe-precursor (Cp_2Fe) flow rate from 50 to 350 standard cubic centimeters per minute (sccm).[7] In the Si-doped (Ga,Fe)N structures the Si content is estimated to be 1×10^{19} cm^{-3}. The growth rate during deposition is regulated by the Ga-precursor trimethylgallium (TMGa) flow rate and varies from 0.08 nm/s for 5 sccm to 0.3 nm/s for 12 sccm of TMGa flow.

B. Experiments and data analysis

The XAFS measurements at the Fe-K edge (7112 eV) are carried out at the "GILDA" Italian collaborating research group beamline (BM08) at the European Synchrotron Radiation Facility in Grenoble.[19] The monochromator is equipped with a pair of Si(111) crystals and run in dynamical focusing mode.[20] Harmonics rejection is achieved by using a pair of Pd-coated mirrors with an estimated cutoff of 18 keV. Data are collected in the fluorescence mode (normal geometry) using a 13-element hyperpure Ge detector and normalized by measuring the incident beam with an ion chamber filled with nitrogen gas. In order to minimize the effects of coherent scattering from the substrate, the samples are mounted on a vibrating sample holder[21] and measurements are carried out at liquid nitrogen temperature to reduce thermal disorder. For each sample the integration time for each energy point and the number of acquired spectra are chosen in order to collect $\approx10^6$ counts on the final averaged spectrum. In addition, before and after each measurement a metallic Fe-reference foil is measured in transmission mode to check the stability of the energy scale and to provide accurate calibration. In this way we locate at 7112.0 eV the first inflection point of the absorption spectrum.[22]

The EXAFS signal, $\chi(k)$, is extracted from the absorption raw data, $\mu(E)$, with the VIPER program[23] employing a smoothing spline algorithm and choosing the energy edge value (E_0) at the maximum derivative. The quantitative analysis is carried out with the IFEFFIT-ARTEMIS programs[24,25] with the atomic models described below. Theoretical EXAFS signals are computed with the FEFF8.4 code[26] using muffin-tin potentials and the Hedin-Lunqvist approximation for their energy-dependent part. The free-fitting parameters used in the analysis are: S_0^2 (common amplitude parameter), ΔE_0 (the refinement of the edge position), R_i and σ_i^2, the interatomic distance, and the Debye-Waller factor for the i^{th} atomic shell around Fe, respectively. In addition, a linear combination parameter (X) is fitted when two theoretical models are used in the same fit. The fits are carried out in the Fourier-transformed space (R space) in the range [1.3–3.5] Å from the k^2-weighted EXAFS data in the range [2.5–10.5] $Å^{-1}$ using Hanning windows with slope-parameter $dk=1$ and $dR=0.1$, for the forward and backward Fourier transforms, respectively. In order to reduce the variables used in the fit and keep the theoretical models coherent for all samples, the fits are limited to $R=3.5$ Å. In fact, the substitutional site in the wurtzite lattice can be reduced to two average distances of Fe-N and Fe-Ga and for ϵ-Fe_3N to the two average distances Fe-N and Fe-Fe. In addition, for simplicity, only one average Fe-N distance is reported in the text. On the other hand, for samples that present only the substitutional phase it is possible to expand the model to upper distances including multiple-scattering (MS) contributions (as pointed out, for example, in the *wurtzite phase analysis* section of Ref. 27) but the results are found to be equivalent. In the case of mixed phases, the expansion to longer distances and MS paths reduces considerably the overall quality of the fits due to the lack of a model compound for ϵ-Fe_3N.

The XANES spectra are normalized using the ATHENA program,[25] setting the edge jump value to unity. The peaks appearing in the energy region before the edge are analyzed with the FITYK program[28] to a curve consisting in an arctangent background[29] plus one or two pseudo-Voigt peaks.[30,31]

C. Theoretical methods

The properties of a Fe atom substituting a Ga atom in GaN (Fe_{Ga}) as well as of the ϵ-Fe_3N hexagonal phase are investigated by density functional theory (DFT) methods by using both the local spin-density generalized gradient approximation (LSD-GGA) (Ref. 32) and the LSD-GGA+U formalism[33] in its rotationally invariant form. The LSD-GGA+U approach, as implemented with plane-wave basis sets in QUANTUM-ESPRESSO,[34–36] has been employed in order to take into account the strong localization of the d states of Fe, poorly described by LSD-GGA exchange-correlation functionals. Considering Hubbard U as an intrinsic property of the atom rather than a fittable parameter is the main difference of such an approach with respect to similar ones (e.g., see Ref. 37). Total energies are calculated in a

supercell approach, by using ultrasoft pseudopotentials[38] plane-wave basis sets, the special-points technique for **k**-space integration, and the Perdew-Burke-Ernzerhof (PBE) exchange-correlation functional.[32]

In detail, for Fe_{Ga} the (1,1,1) **k**-point Monkhorst-Pack mesh for a 72-atom wurtzite supercell of GaN (corresponding to $3\times3\times2$ unit cells), a Gaussian smearing of the occupation numbers and plane-waves cutoffs of 25 Ry for wave functions and 150 Ry for densities are used. The electronic channels considered in the atomic pseudopotentials are $2s$ and $2p$ for N; $3s$, $3p$, $3d$, $4s$, and $4p$ for Fe; and $3d$, $4s$, and $4p$ for Ga. One substitutional Fe atom is included in the 72-atom supercell of GaN. A neutralizing background charge is imposed when dealing with charged states of Fe_{Ga}. Geometry optimizations are performed by fully relaxing the positions of all the supercell atoms by minimizing the atomic forces. The spin state of the system is self-consistently determined during the wave-function optimization. The position of electronic levels induced by the Fe impurity in the GaN energy gap is estimated by calculating the corresponding transition energy levels $\epsilon^{n/n+1}$, that is, the Fermi-energy values for which the charge of the defect changes from n to $n+1$; this gives the position of the Fermi energy (E_F) with respect to the top of the valence band. These values are estimated from total energies (defect-formation energies) as described in Refs. 39 and 40, where further details on the theoretical methods can be found. Transition energy values have to be located with respect to the GaN energy gap. Such an energy gap is estimated here by the $\epsilon^{0/-1}$ transition level relative to bulk GaN in order to compare defect-transition levels and energy gaps calculated in a consistent way.[41] Our estimate of the energy gap, although based on total-energy differences, is affected indeed by the LDA limits which, however, are expected to affect at a comparable extent the estimates of both the defect levels and the energy gap. This should permit a discussion of the Fe electronic properties at a reasonable degree of accuracy. Kohn-Sham electronic eigenvalues at the Γ point and electronic density of states (DOS) are also considered when discussing the electronic properties of the Fe_{Ga} impurity.

In the case of ϵ-Fe_3N, the starting point of the calculations is the hexagonal phase as found in literature on the nitridation process of Fe.[42,43] The space group is $P6322$ (No. 182) with the unit cell composed of six Fe atoms in the Wickoff site $6g$ [$(x,0,0)$; $(0,x,0)$; $(-x,-x,0)$; $(-x,0,1/2)$; $(0,-x,1/2)$; and $(x,x,1/2)$] where $x=0.333$ and two N in site $2c$ [(1/3,2/3,1/4); (2/3,1/3,3/4)]; that is, iron atoms show the motif of a slightly distorted hexagonal close packing (hcp) structure and nitrogen atoms occupy only corner-sharing octahedra (Fig. 7 in Ref. 43). Satisfactorily convergent results are achieved by using the (12,12,8) **k**-point Monkhorst-Pack mesh, plane-wave cutoffs of 35 Ry for wave functions, and 140 Ry for densities.

III. RESULTS

A. Solubility limit as a function of Fe content

The first series systematically studied consists of samples prepared each with different Fe content (Cp_2Fe from 150 to 350 sccm) at a fixed growth rate (TMGa=5 sccm). The recent investigation by HRTEM[48] shows on this series a solubility limit at 200 sccm at our growth conditions. This means that after this limit precipitates appear mostly as ϵ-Fe_3N and, only at the surface of selected samples, as α-Fe. In Fig. 1 are plotted the k^2-weighted EXAFS data where qualitative differences are clearly visible and are highlighted by the peaks A, B, and C. In particular, three different spectra are visible: for 150 sccm, for 200 and 250 sccm, and for 300 and 350 sccm. This difference is also found in the Fourier-transformed (FT) spectra shown in Fig. 2 where, in the range $R_{min}-R_{max}$, from a two-peaks situation (R_1 and R_3) at 150 sccm, an intermediate third peak (R_2) appears and increases in amplitude with increasing Fe content.

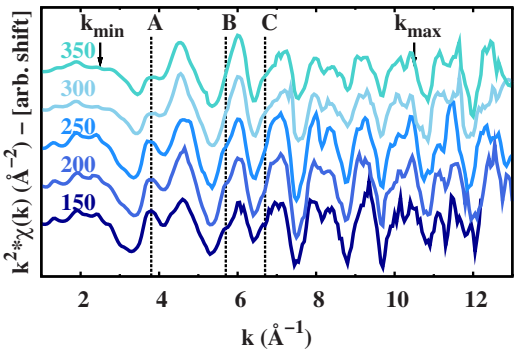

FIG. 1. (Color online) k^2-weighted EXAFS signals for (Ga,Fe)N samples at TMGa=5 sccm as a function of Cp_2Fe content (sccm, labels on spectra); vertical dashed lines highlight some parts of the spectra as described in Sec. III A; k_{min} and k_{max} delimit the Fourier-transformed part of the spectrum used in the fit.

In the quantitative fit, the data at 150 sccm can be reproduced with a two-shell model consisting in a Fe-N (R_1) and Fe-Ga (R_3) shells. The intermediate peak (R_2) is obtained with a Fe-Fe shell. The numerical results are shown in Table I(A).

B. Fe incorporation dependence on growth rate

The second series studied permits to investigate how the

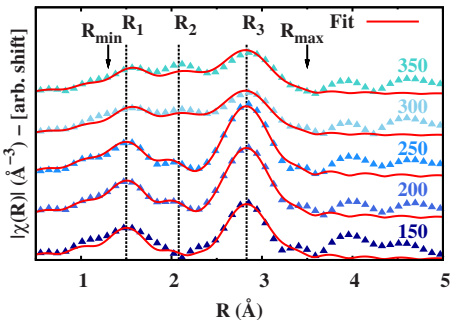

FIG. 2. (Color online) Amplitude of the FT for spectra shown in Fig. 1 with relative fits. R_{min} and R_{max} delimit the fit region; R_1, R_2, and R_3 (with relative dashed vertical lines) indicate the main average distances found in the fit. The R scale has no phase correction (Ref. 47).

TABLE I. Results of the EXAFS quantitative analysis for the (A) first (Ga,Fe)N series at TMGa=5 sccm, the (B)second (Ga,Fe)N series at Cp_2Fe=300 sccm, and the (C) third (Ga,Fe)N:Si series as a function of both TMGa and Cp_2Fe; for clarity only average distances are reported. The values of S_0^2 and ΔE_0 are stable, in the limit of error bars, at 0.9(1) and 6(3) eV, respectively. (D) Averaged crystallographic distances are also reported from literaturefor comparison; in GaN,[44] the Ga-N and Ga-Ga distances are, respectively, 1.95 and 3.18 Å. (E) The last part of the table reports LSD+U atomic distances calculated as described in the text. Errors on the last significative digit are given in brackets (Ref. 45).

		Fe-N		Fe-Fe		Fe-Ga		
Cp_2Fe (sccm)	TMGa (sccm)	R_1 (Å)	σ_1 (10^{-3} Å^{-2})	R_2 (Å)	σ_2 (10^{-3} Å^{-2})	R_3 (Å)	σ_3 (10^{-3} Å^{-2})	X (%)
				(A) (Ga,Fe)N as function of Fe flow rate				
150	5	2.02(1)	6(2)			3.18(1)	6(2)	100(10)
200	5	1.98(1)	7(1)	2.71(3)	19(5)	3.19(1)	7(1)	70(10)
250	5	1.98(1)	7(1)	2.70(3)	22(5)	3.19(1)	7(1)	70(10)
300	5	2.01(2)	8(1)	2.74(3)	21(2)	3.21(2)	8(1)	50(10)
350	5	2.02(3)	7(2)	2.75(4)	21(2)	3.22(2)	7(2)	40(10)
				(B) (Ga,Fe)N as function of Ga flow rate				
300	5	2.01(1)	9(1)	2.75(2)	28(2)	3.23(1)	9(1)	50(10)
300	8	1.98(2)	12(4)			3.19(1)	9(1)	100(10)
300	10	1.97(1)	8(3)			3.19(1)	7(1)	100(10)
300	12	1.97(1)	13(5)			3.19(1)	8(1)	100(10)
				(C) (Ga,Fe)N:Si				
300	5	1.99(2)	13(3)			3.19(1)	9(1)	100(10)
300	10	1.98(2)	9(2)			3.18(1)	7(1)	100(10)
250	10	1.99(2)	14(3)			3.18(1)	8(1)	100(10)
100	10	2.01(3)	11(4)			3.19(1)	9(1)	100(10)
				(D) Crystallographic				
ϵ-Fe_3N [a]		1.927(1)		2.703(2)				
α-Fe [b]				2.499/2.886				
				(E) DFT				
ϵ-Fe_3N		1.89(1)		2.67(1)				
Fe_{Ga}^{+1}		1.97(1)				3.23(1)		
Fe_{Ga}^{0}		1.99(1)				3.22(1)		
Fe_{Ga}^{-1}		2.05(1)				3.21(1)		

[a]Reference 43.
[b]Reference 46

Fe incorporation changes with the growth rate. In fact, by fixing the Fe content at 300 sccm (i.e., well above the solubility limit estimated to be about 200 sccm), the TMGa flow rate is increased from 5 to 12 sccm through the samples series. The EXAFS spectra for this series are shown in Fig. 3 and their respective FTs in Fig. 4. From a qualitative point of view we note that for high growth-rate values (TMGa $\geq$8 sccm) the EXAFS signal consists in two main frequencies (relative to the distances R_1 and R_3 in the FT) whereas in samples grown below that limit a further phase is detected and revealed by the peak R_2. Also in this case the quantitative analysis is conducted by reproducing data either with a substitutional model or with a combination of substitutional plus ϵ-Fe_3N phase. The results are reported in Table I(B).

C. Si codoping

Finally, the effect of codoping with Si is investigated in a samples series with variable TMGa and Cp_2Fe. EXAFS spectra as a function of both TMGa and Cp_2Fe are reported in Fig. 5 with their relative FTs in Fig. 6. By considering the same part of the spectra highlighted in the previous two series, it is visible in this case that no differences emerge between spectra[49] and all present a typical Fe_{Ga} signal. The Fe

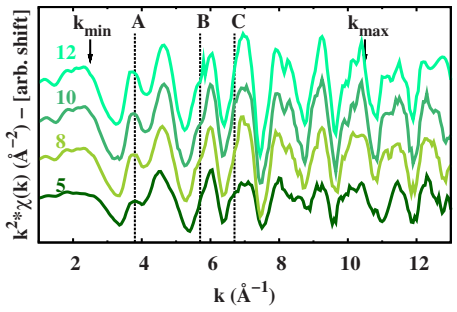

FIG. 3. (Color online) k^2-weighted EXAFS signals for (Ga,Fe)N samples at $Cp_2Fe=300$ sccm as a function of TMGa flow rate (sccm, labels on spectra); vertical dashed lines highlight some parts of the spectra as in Fig. 1; k_{min} and k_{max} delimit the Fourier-tranformed part of the spectrum used in the fit.

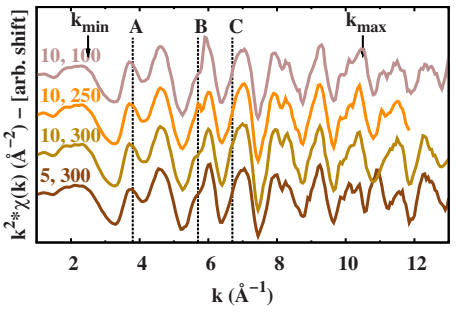

FIG. 5. (Color online) k^2-weighted EXAFS signals for (Ga,Fe)N:Si samples as a function of TMGa and Cp_2Fe (sccm, labels on spectra); vertical dashed lines highlight some parts of the spectra as in Figs. 1 and 3; k_{min} and k_{max} delimit the Fourier-tranformed part of the spectrum used in the fit.

full inclusion in substitutional sites is confirmed by the quantitative analysis reported in Table I(C).

D. Fe charge state

In order to get information on the charge state of Fe in the studied samples, the near-edge region of the absorption spectra (XANES) is analyzed. The amplitude and position of the peaks due to the partially forbidden $1s \rightarrow 3d$ transitions appearing in the pre-edge region of the absorption coefficient were widely investigated in literature as a function of the local symmetry (tetrahedral or octahedral) and valence state (Fe^{3+} or Fe^{2+}) in Fe compounds.[30,31] The general finding was that tetrahedrally coordinated compounds exhibit a single pre-edge peak with an amplitude above 10% of the total edge jump and a position changing with the valence state from $\approx$7112 eV in the case of Fe^{2+} to $\approx$7114 eV in the case of Fe^{3+}.[30]

Here we present a systematic extension of a previous investigation.[9] Quantitative results are reported in Table II, and two representative fits are plotted in Fig. 7; undoped samples exhibit only a single peak of average amplitude $13 \pm 1\%$ and positon 7113.9 ± 0.1 eV whereas the doped samples present the same peak at 7113.9 ± 0.1 eV with a slightly lower average amplitude of $10 \pm 1\%$ and a further peak at 7112.8 ± 0.1 eV of amplitude $3 \pm 1\%$. These data are explained by the presence of Fe^{3+} ions in the first series and a coexistence of Fe^{3+} and Fe^{2+} ions in the second case. The appearance of double peaks in the pre-edge region in case of coexistence of chemical species at different valence states was already pointed out in literature[50,31] and in our case evidences the partial reduction in the metal ions ($Fe^{3+} \rightarrow Fe^{2+}$) upon Si addition.

E. Theoretical results

1. Substitutional Fe in GaN

The local structure of a Fe_{Ga} in GaN is investigated through geometry-optimization procedures both in the LSD and LSD+U frameworks. The estimated lattice constants of the 72-atom supercell are $a=9.66$ Å and $c=10.49$ Å. Details of the atomic geometries produced by the (more reliable) LSD+U calculations are given in Table I(E) for the charge states 0, +1, and −1 of Fe_{Ga}, which correspond to the Fe_{Ga}^{3+}, Fe_{Ga}^{4+}, and Fe_{Ga}^{2+} forms of the impurity, respectively. Present results show that the Fe_{Ga}-N-bond distances for the −1 (+1) state are slightly longer (almost the same) with respect to those of the neutral state. Moreover, no significant differences are found between the Fe_{Ga}-Ga distances estimated for the above three charge states of Fe_{Ga}. A quite simi-

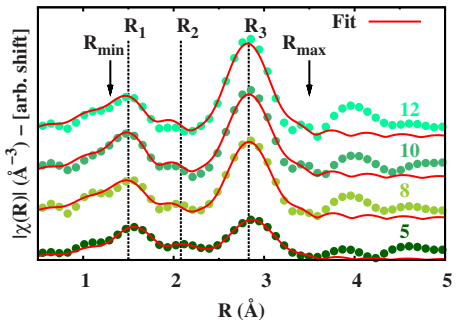

FIG. 4. (Color online) Amplitude of the FT for spectra shown in Fig. 3 with relative fits. R_{min} and R_{max} delimit the fit region; R_1, R_2, and R_3 (with relative dashed vertical lines) indicate the main average distances found from the fit. The R scale has no phase correction (Ref. 47).

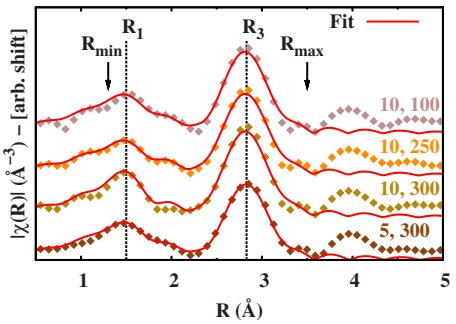

FIG. 6. (Color online) Amplitude of the FT for spectra shown in Fig. 5 with relative fits. R_{min} and R_{max} delimit the fit region; R_1 and R_3 (with relative dashed vertical lines) indicate the main average distances as in Figs. 2 and 4. The R scale has no phase correction (Ref. 47).

TABLE II. Quantitative results of the XANES analysis.

		Peak I		Peak II	
Cp_2Fe (sccm)	TMGa (sccm)	Center (eV)	Height (%)	Center (eV)	Height (%)
		(Ga,Fe)N			
300	5	7113.8(1)	8(1)		
300	8	7113.9(1)	12(1)		
300	10	7113.9(1)	14(1)		
300	12	7113.9(1)	17(1)		
		(Ga,Fe)N:Si			
300	5	7113.9(1)	10(1)	7112.9(1)	2(1)
300	10	7113.9(1)	11(1)	7112.9(1)	3(1)
250	10	7113.9(1)	11(1)	7112.7(1)	3(1)
100	10	7113.8(1)	9(1)	7112.5(1)	4(1)

lar picture is provided by the LSD calculations.

Regarding the electronic properties of Fe_{Ga}, total-spin DOS, and spin DOS projected on the Fe atomic orbitals as given by the LSD+U calculations for the neutral state of the impurity are reported in Fig. 8 together with the calculated Fermi energy. These DOS have to be considered together with an estimate of 1.7 eV given by the Kohn-Sham electronic eigenvalues for the GaN energy gap (E_g). Then, Fig. 8 shows that occupied electronic states induced by the substitutional Fe are mixed with GaN states at the top of the valence band (TVB), whereas unoccupied Fe states are resonant with the conduction band. As discussed in Sec. II C, being aware that the LDA underestimates the gap value instead of determining the position of Fe-related levels from the computed density of states, information on the location of the levels induced by a Fe_{Ga} in the GaN energy gap is obtained by calculating the corresponding $\epsilon^{0/-1}$ transition level where the Fe impurity changes its charge state from 0 to −1. The present evaluation of the $\epsilon^{0/-1}$ level is 2.25 eV to be compared with a calculated E_g of 2.93 eV. These results favorably compare with the experimental findings locating the Fe acceptor level at 2.86 eV,[51] on a band gap of 3.50 eV for wz-GaN at 0 K.[52] It can be noted that an even better agreement with the experiment can be reached by assuming a linear scaling of $\epsilon^{0/-1}$ with the energy gap, leading to $\bar{\epsilon}^{0/-1} = \epsilon^{0/-1} E_g^{(\mathrm{exp})} / E_g = 2.7$ eV.

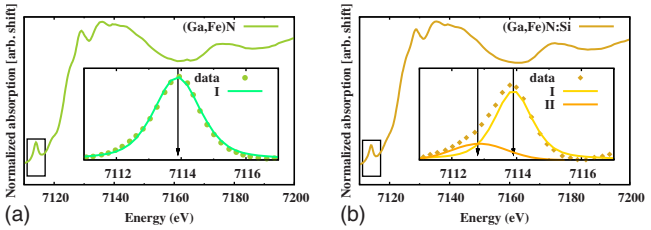

FIG. 7. (Color online) Normalized XANES spectra for (Ga,Fe)N (left) and (Ga,Fe)N:Si (right) with the prepeak reported in the inset after baseline subtraction and the fitted functions with centroids indicated by arrows.

The present results agree with a deep acceptor character of Fe_{Ga}. They seem also to rule out a possible donor behavior of Fe_{Ga}. In Fig. 8 it is shown indeed that there are no occupied Fe states in the GaN energy gap. Moreover, a value of −0.03 eV has been estimated for the $\epsilon^{0/+1}$ transition level indicating that a $Fe^{3+/4+}$ donor level of Fe_{Ga} would be resonant with the valence band. In agreement with this conclusion no such state has been found experimentally in the band gap of GaN:Fe.[53] However, the present *ab initio* findings do not rule out a possibility that the Fe impurity in GaN gives rise to a charge-transfer state, $Fe^{3+}+h$, acting as a hole trap, as postulated by some of us.[8,54]

The results of the present calculations permit also to assess a change in the formation energies of Fe_{Ga} in different charge states (Ω_F^q) as a function of the Fermi-energy E_F. For instance, for the magnitude of Ω_F^{-1}-Ω_F^0, we estimate +0.68 and −0.78 eV for E_F equal to $E_g/2$ and E_g, respectively (these values are calculated by using our estimate of E_g). This indicates that the formation of Fe_{Ga}^{3+} is promoted in intrinsic GaN, while Fe_{Ga}^{2+} is favored in the n-doped material.

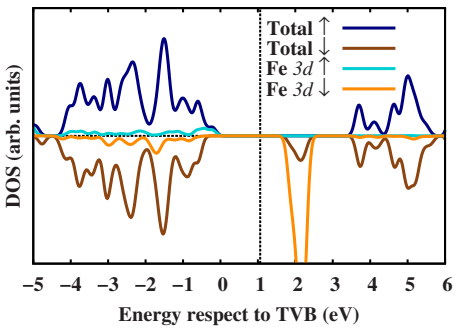

FIG. 8. (Color online) LSD+U total spin DOS and DOS projected on the Fe atomic orbitals for a substitutional Fe in the neutral charge state. The DOS for Fe are magnified ten times for sake of clarity. The position of the Fermi energy is indicated by a vertical dashed line and shown in respect to the top of the valence band (TVB). The calculated absolute value of the Fermi energy (E_F) is 10.52 eV.

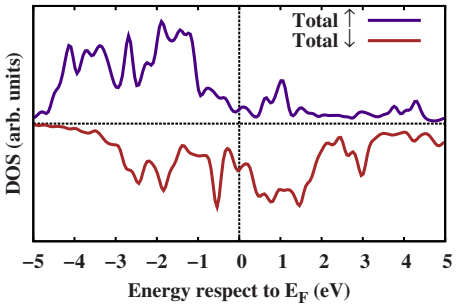

FIG. 9. (Color online) LSD total spin DOS for ϵ-Fe_3N. The position of the Fermi energy (E_F) is indicated by a vertical dashed line. The calculated absolute value of E_F is 17.64 eV.

On the contrary, the value of Ω_F^{+1}-Ω_F^0 is evaluated as +0.10 and +1.57 eV for the Fermi level at the top of the valence band and in the middle of the energy gap, respectively, that is, a donor behavior of Fe (corresponding to the formation of Fe_{Ga}^{4+}) is never favored.

2. ϵ-Fe_3N

The cell parameters are calculated by minimizing the total energy of the system. Optimal values are found at the zero value of linear fits of the total stress, corresponding to the minimum of the total energy. Such a procedure gives a =4.64 Å and c=4.34 Å, that is, ≈2% contraction of the experimental values a_{exp}=4.7209(6) Å and c_{exp} =4.4188(9) Å; this being a typical effect of the LSD approximation. The relaxation properly reproduces the experimental value of x that is a 0.009 contraction from the 1/3 ideal value of x for Fe in the hcp structure. The resulting atomic distances reported in Table I(E) are slightly different from the crystallographic ones[43] [Table I(D)]. The above structural minimization corresponds to a magnetization of 2.2 μ_B/atom, in agreement with the experimental value found from neutron diffraction at 4.2 K.[55] Finally, the total DOS shown in Fig. 9 gives a clear evidence of the metallic behavior of this system. These results are achieved by LSD calculations; the LSD+U scheme is also tested with different U values in the range 2–5 eV and no appreciable difference is found between the LSD and LSD+U results.

IV. DISCUSSION

A. EXAFS

In the first series presented in this study the sample with a lower Fe content exhibits two coordination shells around Fe. These shells are identified as Fe-N and Fe-Ga contributions and the observed bond-length values are in agreement with those calculated via DFT for a Fe ion in a Ga-substitutional site. Thus, we conclude that Fe substitutes Ga, as previously suggested by a qualitative analysis of EXAFS data.[56] The closeness of the theoretical estimates of the Fe-N distances reported in Table I(E) makes it difficult to exploit the Fe_{Ga} local geometry to distinguish between its possible, different charge states. However, the theoretical results support a deep acceptor character of Fe_{Ga} and locate the corresponding electronic level in the upper half of the GaN energy gap. Accordingly, the Ω_F^0 formation energy is 0.40 eV lower in energy than Ω_F^{-1} in intrinsic GaN, thus suggesting the presence of Fe_{Ga} in the neutral state.

For samples grown with higher Fe content an additional shell appears, matching a coordination at 2.70–2.75 Å. This value coincides with the experimental and calculated Fe-Fe second shell distance in ϵ-Fe_3N. This suggests that Fe precipitates in the form of ϵ-Fe_3N. It is worth noting that in this compound the first shell corresponds to the Fe-N bonds exhibiting the same structural parameters (length and number of neighbors) as those specific to Ga-substitutional Fe in GaN. These results provide an independent confirmation of our previous studies on (Ga,Fe)N,[7,48] according to which Fe-rich nanocrystals were evidenced by neither HRTEM nor high-resolution x-ray diffraction (HRXRD) and a paramagnetic response was observed by superconducting quantum interference device (SQUID) in samples with a low Fe content, whereas samples with a high Fe content showed the presence of Fe-rich nanocrystals and a ferromagnetic behavior.

From a reduction in the amplitude of the dominating Fe-Ga signal relative to the pure substitutional specimen it is possible to estimate the relative content of Fe in the two phases (GaN and ϵ-Fe_3N), as shown in Table I. From these data we infer that the flow rate of 200 sccm Cp_2Fe corresponds to the onset of ϵ-Fe_3N precipitation at our growth conditions, though the spinodal decomposition that is the aggregation of Fe cations without crystallographic phase separation may begin at lower Fe contents. Significantly, no presence of ϵ-Fe_3N is detected in samples codoped with Si.

It is worth to underline that no evidence is found for the α-Fe phase that should be witnessed by a double Fe-Fe shell at 2.499 and 2.886 Å.[46] Actually, this phase was shown to be present only at the surface of samples grown under particular conditions[48] and the overall Fe fraction in this phase presumably lies below the detection limit of EXAFS (about 15% in the present case).

We also observe that our data do not point to the presence of Fe in interstitial sites, at least in samples containing no secondary phases, for which the EXAFS signal is completely reproduced by a simple substitutional model. In the case of samples with precipitates, their contribution could *a priori* mask a signal coming from interstitials. This is in contrast to the case of (Ga,Mn)As where evidence for Mn interstitials has been found in EXAFS studies.[15,16]

Turning to samples deposited at different growth rates we note that if the Fe content exceeds the previously determined solubility limit, we find again the presence of ϵ-Fe_3N nanocrystals in the film grown at the lowest rate (TMGa =5 sccm). For faster growth rates, however, the EXAFS spectra correspond exclusively to substitutional Fe_{Ga} in GaN, emphasizing the effectiveness of the fast growth in suppressing the formation of segregated phases. This observation is in qualitative agreement with the previous study,[57] where HRTEM carried out for samples grown at low and high rates (although at a noticeably higher Fe content) revealed the formation of ϵ-Fe_3N only for slowly grown specimens.

B. XANES

The XANES spectral region is characterized by the presence of a single pre-edge peak at about 7114 eV in all samples grown without Si. In agreement with the literature data[30,31,50] this reveals that Fe assumes the Fe^{3+} charge state in a tetrahedral environment, and this result corroborates the conclusions derived from previous electron paramagnetic resonance studies[7,53] and from the present DFT calculation for (Ga,Fe)N. Codoping with Si results in the appearance of an additional peak in the pre-edge region at about 7112.8 eV, which is attributed to Fe^{2+} ions in a tetrahedral environment, as already pointed out in our prior work.[9] The fraction of the total Fe content in this particular valence state is below 20%, the majority of Fe impurities still remaining in the Fe^{3+} configuration. This explains why we do not observe in the EXAFS data (and, in particular, in the values of the Fe-N bond length) any significant deviation when comparing the samples containing no Si impurities with the Si-doped ones. However, the codeposition of Si hampers the aggregation of Fe and, thus, shifts the solubility limit to higher Fe concentrations.

The above interpretation of the XANES findings is consistent with the *ab initio* results, implying that the Fe^{2+}/Fe^{3+} state, i.e., the $\epsilon^{0/-1}$ level, resides in the GaN gap 2.25 eV above the top of the valence band. Thus, this state should be occupied by electrons provided by shallow donors, such as Si. This conclusion is further supported by the computed formation energy that results to be for the Fe^{3+} configuration by 1.35 eV higher than for the Fe^{2+} case.

V. CONCLUSIONS AND OUTLOOK

The present EXAFS results, together with previous HR-TEM, electron dispersive spectroscopy, and synchrotron XRD,[9] show how the Fe incorporation can be efficiently controlled by Fe flow, growth rate, and codoping with Si. In particular, the aggregation of Fe cations can be minimized by increasing the growth rate and by codoping with Si, shifting the solubility limit toward higher Fe content at given growth conditions. While there is agreement between the present DFT computations and both the previously[7,53] and here observed Fe charge state, including its evolution with the Si concentration, a detailed understanding of how codoping and other growth parameters affect the aggregation of Fe ions awaits for a comprehensive theoretical treatment.

A strict correlation between magnetic properties and the presence of Fe-rich nanocrystals[7,9] strongly suggests that the surprisingly robust ferromagnetism of (Ga,Fe)N as well as of other diluted magnetic semiconductors and oxides deposited under specific growth conditions results from the self-organized assembly of magnetic nanocrystals, whose high blocking temperatures account for the survival of ferromagnetic features at high temperatures. This emerging insight provides a promising starting point for exploiting a number of expected functionalities of these nanocomposite semiconductor/ferromagnetic metal systems.[6,58]

ACKNOWLEDGMENTS

We acknowledge the European Synchrotron Radiation Facility and the Italian Collaborating Research Group for the provision of the synchrotron-radiation facilities. GILDA is a project jointly financed by CNR and INFN. M.R. is indebted to Piotr Bogusławski and Paweł Jakubas for valuable discussions during his visit in Warsaw and to CNR for financial support by the Short Term Mobility 2008 program (Contract No. N.0002372). We also acknowledge Federico Boscherini for fruitful discussions. This work has been partly supported by the Austrian Fonds zur Förderung der wissenschaftlichen Forschung (Contracts No. P18942, No. P20065, and No. N107-NAN), by the ESF FoNe project SPINTRA (Contract No. ERAS-CT-2003-980409), and by the FunDMS Advanced Grant within the European Research Council "Ideas" Programme of EC 7FP.

*mauro.rovezzi@esrf.eu

[1] S. Kuroda, N. Nishizawa, K. Takita, M. Mitome, Y. Bando, K. Osuch, and T. Dietl, Nature Mater. **6**, 440 (2007).
[2] S. Chambers, T. Droubay, C. Wang, K. Rosso, S. Heald, D. Schwartz, K. Kittilstved, and D. Gamelin, Mater. Today **9**, 28 (2006).
[3] M. Kobayashi *et al.*, New J. Phys. **10**, 055011 (2008).
[4] A. Bonanni, Semicond. Sci. Technol. **22**, R41 (2007).
[5] T. Dietl, J. Phys.: Condens. Matter **19**, 165204 (2007).
[6] H. Katayama-Yoshida, K. Sato, T. Fukushima, M. Toyoda, H. Kizaki, V. A. Dinh, and P. H. Dederichs, Phys. Status Solidi A **204**, 15 (2007).
[7] A. Bonanni *et al.*, Phys. Rev. B **75**, 125210 (2007).
[8] W. Pacuski *et al.*, Phys. Rev. Lett. **100**, 037204 (2008).
[9] A. Bonanni *et al.*, Phys. Rev. Lett. **101**, 135502 (2008).
[10] P. A. Lee, P. H. Citrin, P. Eisenberger, and B. M. Kincaid, Rev. Mod. Phys. **53**, 769 (1981).
[11] F. Boscherini, *X-ray Absorption Fine Structure in the Study of Semiconductor Heterostructures and Nanostructures* (Elsevier, New York, 2008), Chap. 9, p. 289.
[12] Y. L. Soo, G. Kioseoglou, S. Huang, S. Kim, Y. H. Kao, Y. Takatani, S. Haneda, and H. Munekata, J. Synchrotron Radiat. **8**, 874 (2001).
[13] Y. L. Soo, G. Kioseoglou, S. Kim, S. Huang, Y. H. Kao, S. Kuwabara, S. Owa, T. Kondo, and H. Munekata, Appl. Phys. Lett. **79**, 3926 (2001).
[14] Y. L. Soo, S. Kim, Y. H. Kao, A. J. Blattner, B. W. Wessels, S. Khalid, C. S. Hanke, and C.-C. Kao, Appl. Phys. Lett. **84**, 481 (2004).
[15] R. Bacewicz, A. Twaróg, A. Malinowska, T. Wojtowicz, X. Liu, and J. Furdyna, J. Phys. Chem. Solids **66**, 2004 (2005).
[16] F. d'Acapito, G. Smolentsev, F. Boscherini, M. Piccin, G. Bais, S. Rubini, F. Martelli, and A. Franciosi, Phys. Rev. B **73**, 035314 (2006).
[17] M. Rovezzi, T. Devillers, E. Arras, F. d'Acapito, A. Barski, M. Jamet, and P. Pochet, Appl. Phys. Lett. **92**, 242510 (2008).

[18] T. Dietl, Nature Mater. **5**, 673 (2006).
[19] F. D'Acapito *et al.*, ESRF Newsl. **30**, 42 (1998).
[20] S. Pascarelli, F. Boscherini, F. D'Acapito, J. Hrdy, C. Meneghini, and S. Mobilio, J. Synchrotron Radiat. **3**, 147 (1996).
[21] V. Tullio, F. D'Anca, F. Campolungo, F. D'Acapito, F. Boscherini, and S. Mobilio, *Internal Note* (LNF-INFN, Frascati, 2001).
[22] J. A. Bearden and A. F. Burr, Rev. Mod. Phys. **39**, 125 (1967).
[23] K. V. Klementev, J. Phys. D **34**, 209 (2001).
[24] M. Newville, J. Synchrotron Radiat. **8**, 322 (2001).
[25] B. Ravel and M. Newville, J. Synchrotron Radiat. **12**, 537 (2005).
[26] A. L. Ankudinov, B. Ravel, J. J. Rehr, and S. D. Conradson, Phys. Rev. B **58**, 7565 (1998).
[27] F. Decremps, F. Datchi, A. M. Saitta, A. Polian, S. Pascarelli, A. Di Cicco, J. P. Itié, and F. Baudelet, Phys. Rev. B **68**, 104101 (2003).
[28] M. Wojdyr, see http://www.unipress.waw.pl/fityk/
[29] The function has been parametrized as: $f(x)=a_1\text{atan}[(x-a_2)a_3]+a_4$, where a_1, a_2, a_3, and a_4 are fitted with a Levenberg-Marquardt algorithm.
[30] L. Galoisy, G. Calas, and M. A. Arrio, Chem. Geol. **174**, 307 (2001).
[31] T. E. Westre, P. Kennepohl, J. G. DeWitt, B. Hedman, K. O. Hodgson, and E. I. Solomon, J. Am. Chem. Soc. **119**, 6297 (1997).
[32] J. P. Perdew, K. Burke, and M. Ernzerhof, Phys. Rev. Lett. **77**, 3865 (1996).
[33] V. I. Anisimov, F. Aryasetiawan, and A. I. Lichtenstein, J. Phys.: Condens. Matter **9**, 767 (1997).
[34] M. Cococcioni and S. de Gironcoli, Phys. Rev. B **71**, 035105 (2005).
[35] H. J. Kulik, M. Cococcioni, D. A. Scherlis, and N. Marzari, Phys. Rev. Lett. **97**, 103001 (2006).
[36] P. Giannozzi *et al.*, see http://www.quantum-espresso.org
[37] P. Blaha, K. Schwarz, G. Madsen, D. Kvasnicka, and J. Luitz, *WIEN2K, An Augmented Plane Wave+Local Orbitals Program for calculating Crystal Properties* (Techn. Universität Wien, Austria, 2001).
[38] D. Vanderbilt, Phys. Rev. B **41**, 7892 (1990).
[39] A. Amore Bonapasta, F. Filippone, and P. Giannozzi, Phys. Rev. B **68**, 115202 (2003).
[40] C. G. Van de Walle and J. Neugebauer, J. Appl. Phys. **95**, 3851 (2004).
[41] A. Amore Bonapasta, F. Filippone, and P. Giannozzi, Phys. Rev. B **69**, 115207 (2004).
[42] K. H. Jack, Acta Crystallogr. **5**, 404 (1952).
[43] H. Jacobs, D. Rechenbach, and U. Zachwieja, J. Alloys Compd. **227**, 10 (1995).
[44] H. Schulz and K. H. Thiemann, Solid State Commun. **23**, 815 (1977).
[45] For XAFS results, the error bars are the diagonal elements of the covariance matrix evaluated during the fit and rescaled by the square root of the reduced χ^2. For the DFT method, they are the resulting variance of convergence tests.
[46] H. Swanson and E. Tatge, Natl. Bur. Stand. Circ. (U. S.) **539**, 1 (1955).
[47] The R value shown in the FT of the EXAFS data does not correspond to the real distance, as reported in Table I. This is due to the linearly decreasing dependence of the phase term, $\psi(k)$, in the EXAFS formula (Ref. 10). A shift of $\approx 0.3-0.5$ Å is observed in the present case.
[48] T. Li, C. Simbrunner, A. Navarro-Quezada, M. Wegscheider, M. Quast, D. Litvinov, D. Gerthsen, and A. Bonanni, J. Cryst. Growth **310**, 3294 (2008).
[49] The spectrum (5300) presents a peak at $k=11$ Å^{-1} that is unphysical. It is due to a distortion by diffraction effects (as discussed in the experimental section) and a consequent problematic background removal.
[50] G. Giuli, G. Pratesi, C. Cipriani, and E. Paris, Geochim. Cosmochim. Acta **66**, 4347 (2002).
[51] E. Malguth, A. Hoffmann, W. Gehlhoff, O. Gelhausen, M. R. Phillips, and X. Xu, Phys. Rev. B **74**, 165202 (2006).
[52] B. Monemar, Phys. Rev. B **10**, 676 (1974).
[53] E. Malguth, A. Hoffmann, and M. R. Phillips, Phys. Status Solidi B **245**, 455 (2008).
[54] T. Dietl, Phys. Rev. B **77**, 085208 (2008).
[55] A. Leineweber, H. Jacobs, F. Huning, H. Lueken, H. Schilder, and W. Kockelmann, J. Alloys Compd. **288**, 79 (1999).
[56] Y. Kumagai, F. Satoh, R. Togashi, H. Murakami, K. Takemoto, J. Iihara, K. Yamaguchi, and A. Koukitu, J. Cryst. Growth **296**, 11 (2006).
[57] A. Navarro-Quezada, T. Li, C. Simbrunner, M. Kiecana, G. Hernandez-Sosa, M. Quast, M. Wegscheider, M. Sawicki, T. Dietl, and A. Bonanni, J. Cryst. Growth **310**, 1772 (2008).
[58] T. Dietl, J. Appl. Phys. **103**, 07D111 (2008).